



DESY Summer Student Program



Influence of the oxide thickness on the magnetic properties of Fe/ FeO multilayers.

Student: Guryeva Tatyana

Supervisors: Ralf Röhlsberger
Kai Schlage
Sebastien Couet

Hamburg, 2008

Contents

Introduction.....	3
Magneto-optic Kerr effect.....	3
Experimental setup for multilayer thin film deposition.....	5
Sample preparation.	6
Results.....	7
Conclusions.....	13
References.....	13

Introduction.

At the present time magnetic thin films have a lot of applications in microelectronics, magnetorecording, biology, chemistry and medicine. Magnetic multilayer structure is used in spin valves and magnetic tunnel junctions. Recently, multilayer structure composed of Fe/ native oxide bilayers have been proposed as new compound combining high magnetization and low conductivity [1].

A systematic study of the influence of the thickness of the oxide layer on the magnetic properties of this structures is still absent.

In this work, I investigate 15 bilayer Fe/ Fe native oxide multilayers where the oxygen exposure was varied between 100-1000L ($1\text{L} = 10^{-6} \text{ Torr} \times \text{s}$). The magnetic hysteresis curves of the sample were measured by magneto optical Kerr effect magnetometry.

Magneto-optic Kerr effect.

The Kerr effect results from the interaction between an electromagnetic wave polarized linearly and a magnetized medium. The considered wave is then polarized elliptically.

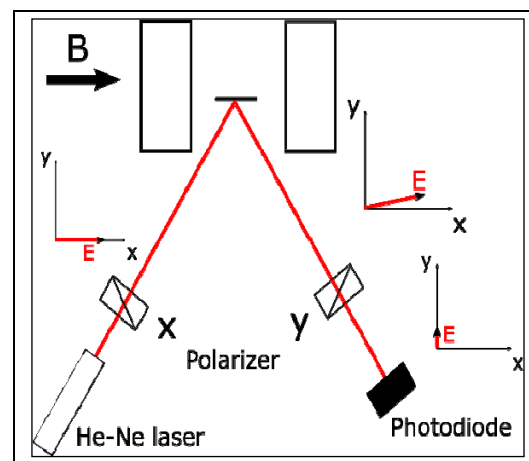


Fig. 1. The experimental setup based on Longitudinal MOKE

Two angles allowing to characterize the elliptic polarization of the light, are defined: Kerr rotation (θ_K) and the Kerr ellipticity (ϵ_K). It can be shown that these two parameters in the case of magnetic thin films are proportional to the magnetization and to the film thickness. An experiment consists in measuring the rotation or the ellipticity according to the intensity of an external field applied in a definite direction that gives an hysteresis loop.

MOKE can be further characterized by the direction of the magnetization vector with respect to the reflecting surface and the plane of incidence.

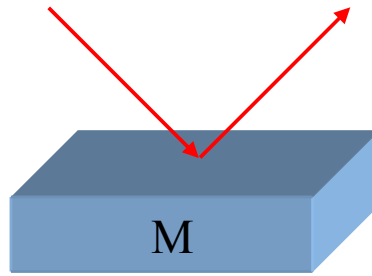


Fig.2. Longitudinal MOKE geometry.

In our case we use setup based on Longitudinal MOKE (Fig. 1). The light of a He-Ne laser ($\lambda=632.8$ nm) in combination with a Glan-Thompson prism is used. The prism and the laser can be rotated and shifted. After the light reflected from the sample, α polarization is analyzed with a second Glan-Thompson prism. An intensity of light is measured after the second prism by a photodiode. The sample is placed between the pole of an electromagnet which can provide a maximum magnetic field of 150 mT .

For longitudinal MOKE, the magnetic field is parallel to both the plane of incidence and the sample surface. (Fig.2)

The longitudinal setup involves light reflected from the sample surface. Linearly polarized light incident on the surface becomes elliptically polarized, with the change in polarization directly proportional to the component of magnetization that is parallel to the reflection surface and parallel to the plane of incidence.

There are two cases of incident polarization that must be considered: the S polarization, where the direction of the linear polarization is normal to the plane of incidence, and the P-polarization, where the plane of polarization and the plane of incidence are parallel. If the first polarizer is placed in a precision rotator, both cases may be studied by simply changing the first polarizer orientation.

Experimental setup for multilayer thin film deposition.

The thin film deposition setup consist of a UHV chamber with main body and load-lock, manipulator, transfer stick and control system (Fig.2).

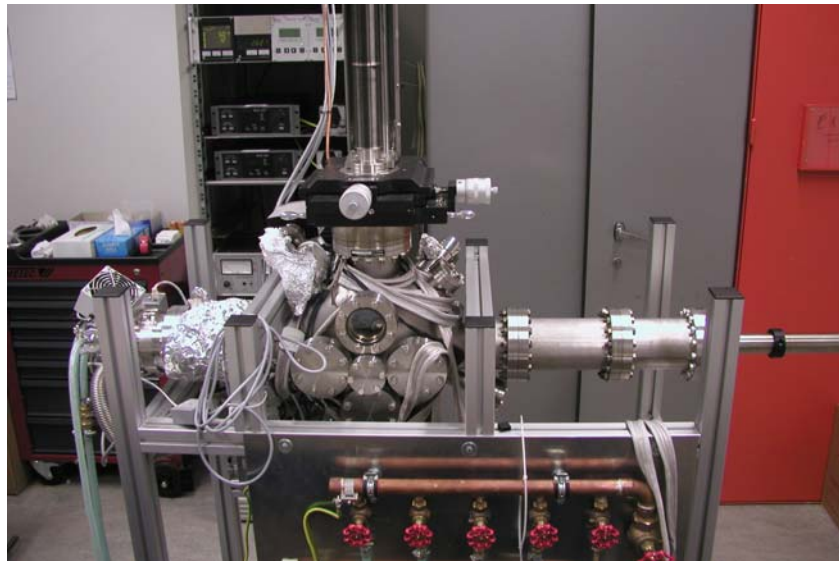


Fig.2 The deposition system.

The main (ultra high vacuum) UHV system is used for thin film preparation. UHV conditions are reached using a two stage turbomolecular, oil free pumping system. This system allows to reach pressure below 5×10^{-9} mbar.

The sample holder is equipped with a specially designed heater stage, developed to perform temperature dependence studies. The holder is placed on 3-axes rotary manipulator.

The deposition system is based on the magnetron sputter deposition. The deposition rate is a function only of the argon gas pressure and of the power of source. The chamber is equipped with three DC magnetron sputter guns. The main deposition source is placed below the sample, at a distance of 63 mm from the sample and fits 33 mm diameter target. At this distance the homogeneity is better than 10% for a 50 mm in diameter sample. Two other sources (25.4 mm) are placed on both sides of the sample with an angle of 35° relative to the sample surface.

The complete setup is controlled by a LABVIEW program (Fig.3). It allows to monitor the systems parameters (pressure, current, voltage, power of sputter sources and oxidation) and change them [2].

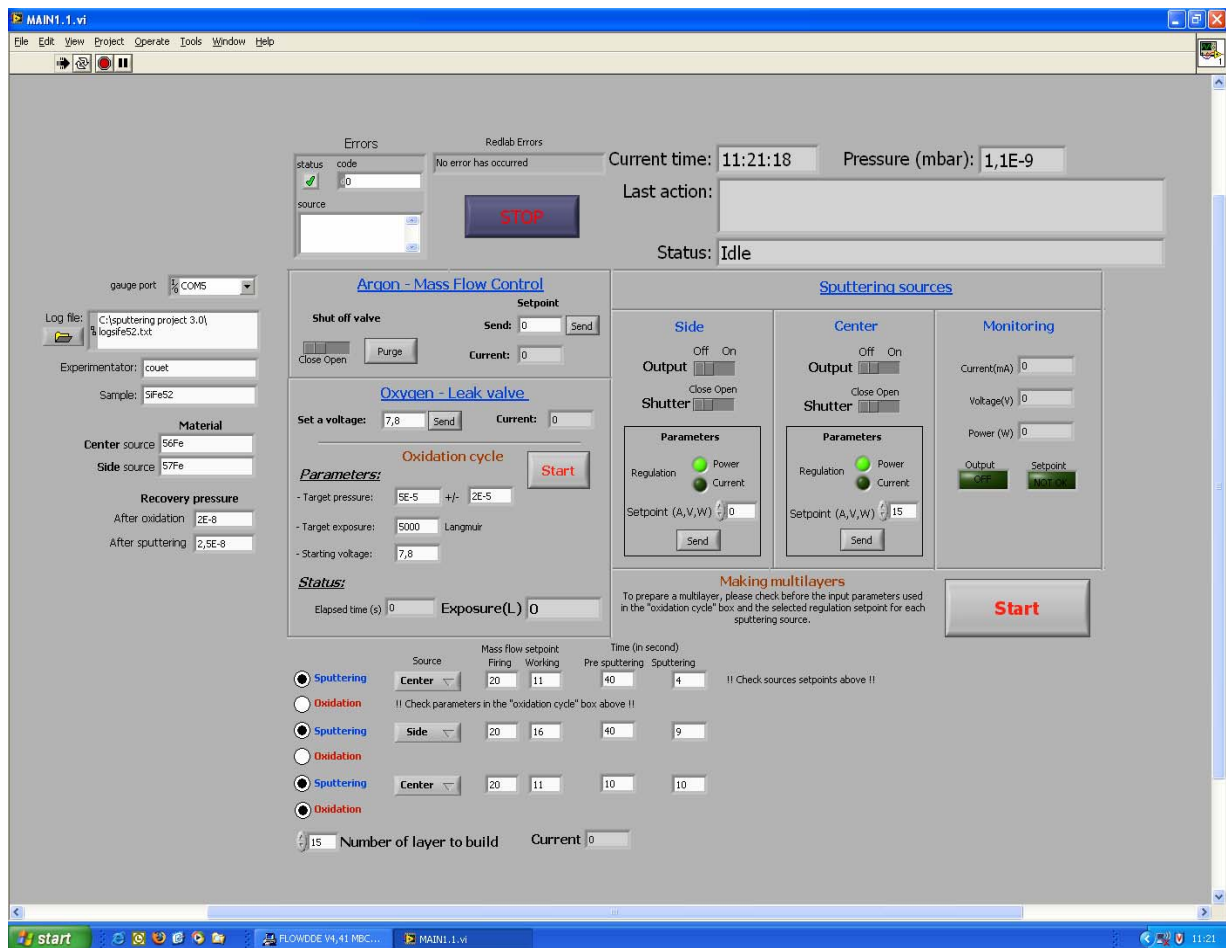


Fig.3 Graphical user interface of control program.

Sample preparation.

Fe/FeO superlattices of 15 bilayers were grown under ultrahigh vacuum (UHV) conditions. First 2.5 nm Fe layer was deposited on Si wafers. The oxide was formed by controlled oxidation. In this case, the total oxygen exposure was varied between 100 and 1000L to grow oxide of different thickness. The films were capped with 4nm of Ta for protection against oxidation. (Fig.4)

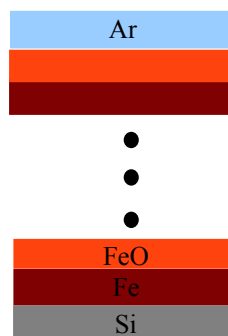


Fig.4 The structure of multilayer magnetic film.

Results.

Hysteresis loops were recorded for each sample using the setup described. The hysteresis loops are measured on two axes (easy and hard), are presented on Fig.5. The loops are different and indicate a small anisotropy of magnetization. The H_c is small for this sample in both cases ($H_{c(e.a.)}=1.75\text{mT}$, $H_{c(h.a.)}=1.05\text{mT}$).

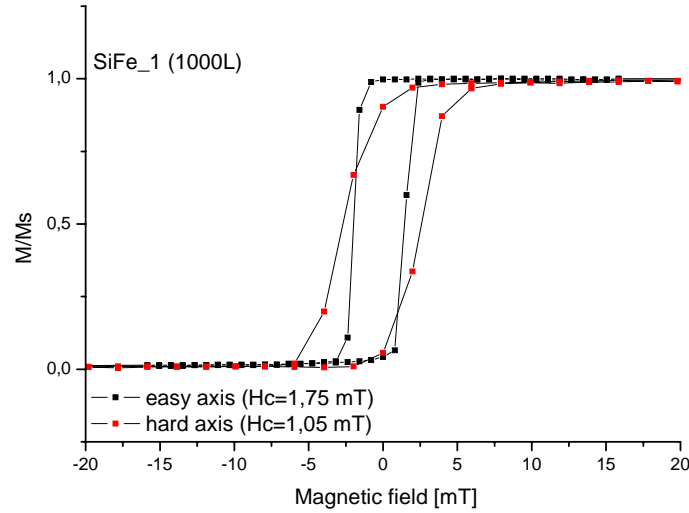


Fig.5 Hysteresis loops for the two axes. The oxygen exposure is 1000L.

The results for 900 exposure are on shown fig. 6. The difference is larger between the two axes. In this case, the easy axis shown observed switching on loop. It can be explain by switching in domain structure. The coercivity increased in both cases ($H_{c(e.a.)}=2.87\text{mT}$, $H_{c(h.a.)}=6.65\text{mT}$), especially in case of hard axis, where is no switching.

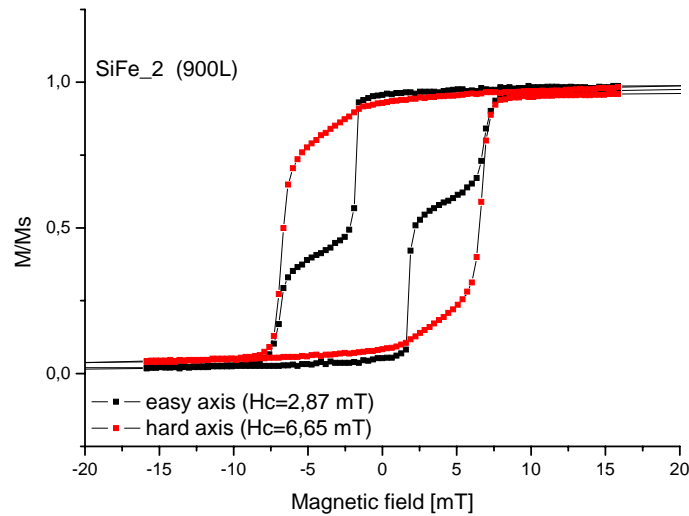


Fig.6 Hysteresis loops for the two axes. The oxygen exposure is 900L.

For the 800L (Fig.7), the loops are similar as for the 1000L case. Some anisotropy is remaining, but feebly marked. The coercivity is less then for 900L ($H_{c(e.a.)}=1.42\text{mT}$, $H_{c(h.a.)}=1.4\text{mT}$).

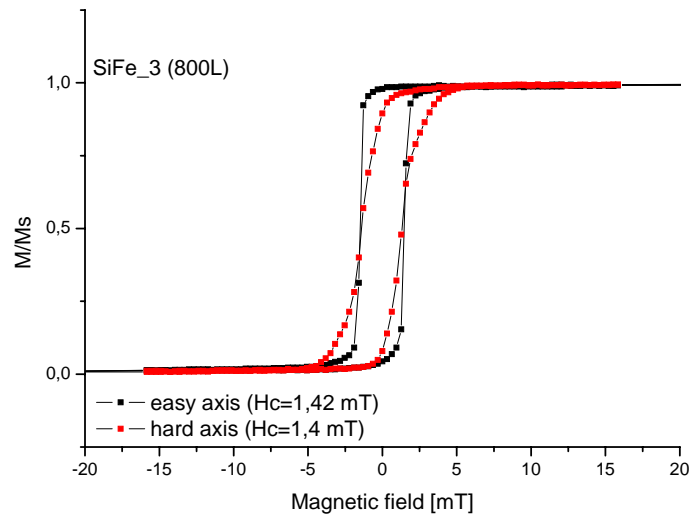


Fig.7 Hysteresis loops for the two axes. The oxygen exposure is 800L.

For 700L and 600L (Fig.8, 9), we can see the asymmetry between the axes disappeared. The coercivity is $H_{c(e.a.)}=3.92,(4.02)\text{ mT}$; $H_{c(h.a.)}=3.75,(3.82)\text{ mT}$.

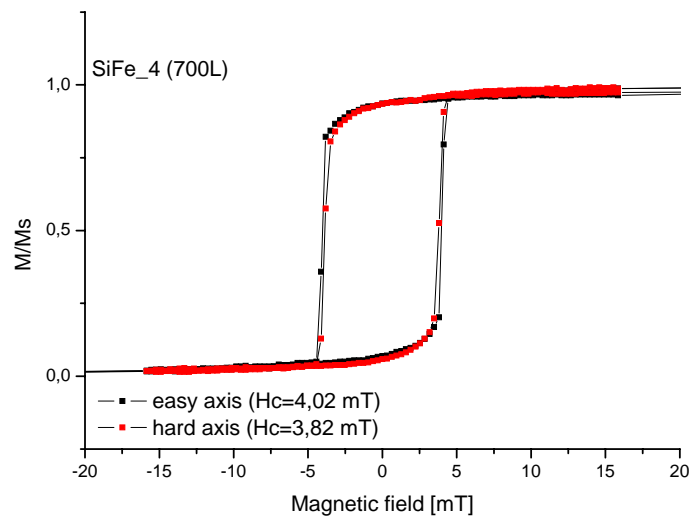


Fig.8 Hysteresis loops for the two axes. The oxygen exposure is 700L.

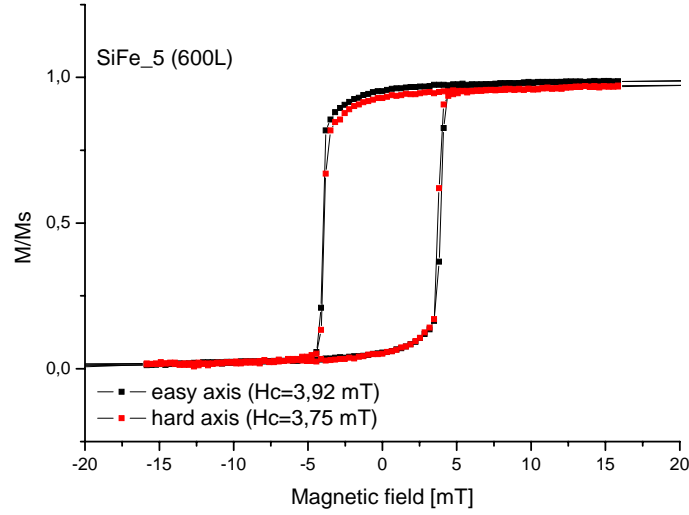


Fig.9 Hysteresis loops for the two axes. The oxygen exposure is 600L.

At 500L (Fig.10) we can observe a second “decrease” of the H_c ($H_{c(e.a.)} = 1.38$ mT, $H_{c(h.a.)} = 0.97$ mT). The asymmetry between different axes appears again and loops are similar to the 1000L and 800L case.

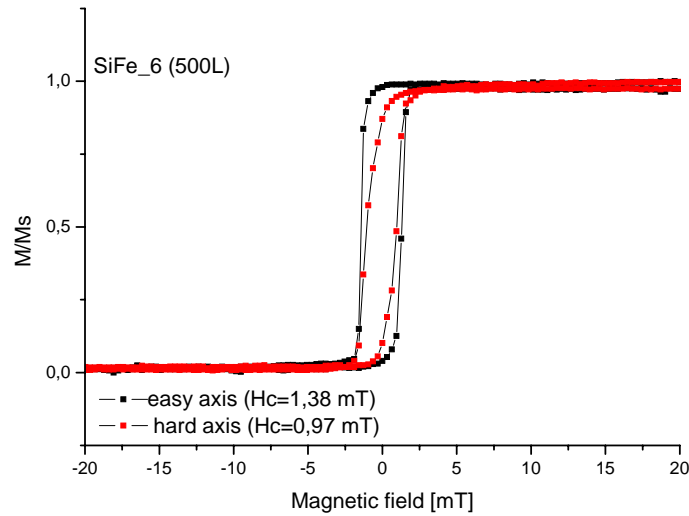


Fig.10 Hysteresis loops for the two axes. The oxygen exposure is 500L.

400L (Fig.11) and 500L (Fig.12) show an evaluation in the switching, but this time about 60% for 400L and 30% for 300L of domains switched. The partial switching takes place in the case of the hard axis (in contrast to 900L (Fig.6)). The H_c increases again ($H_{c(e.a.)} = 5.43(6.5)$ mT, $H_{c(h.a.)} = 3.25(6)$ mT).

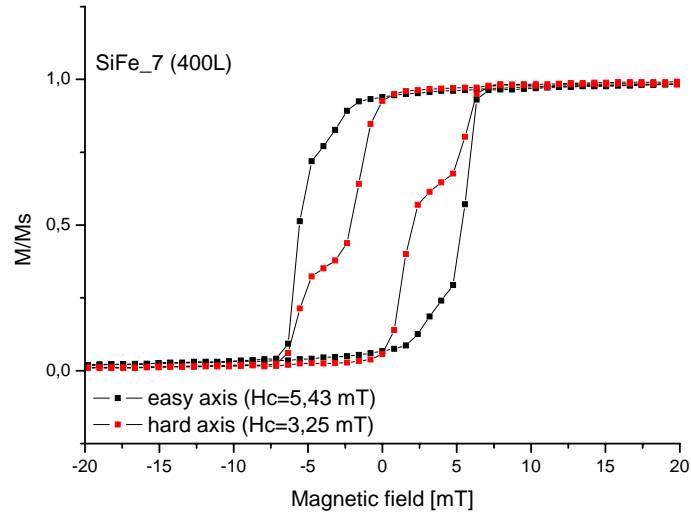


Fig.11 Hysteresis loops for the two axes. The oxygen exposure is 400L.

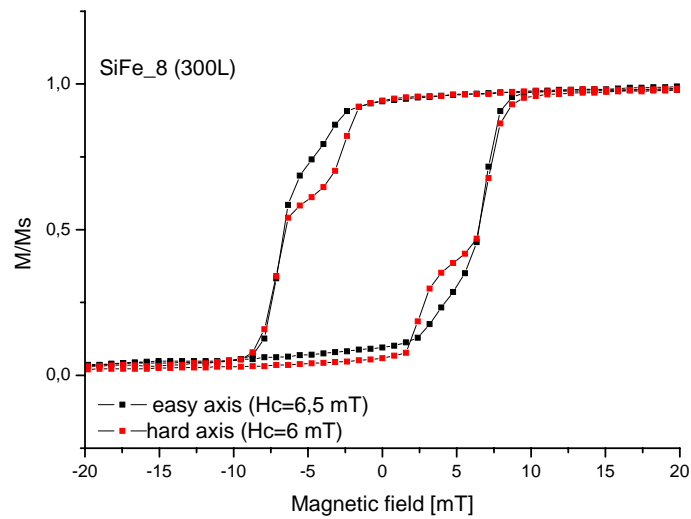


Fig.12 Hysteresis loops for two axes. The oxygen expose is 300L.

At 200L (Fig.13) 100% of the domains switched and both loops are symmetric. The H_c is still large ($H_{c(e.a.)} = 7.45$, $H_{c(h.a.)} = 7.45$ mT)

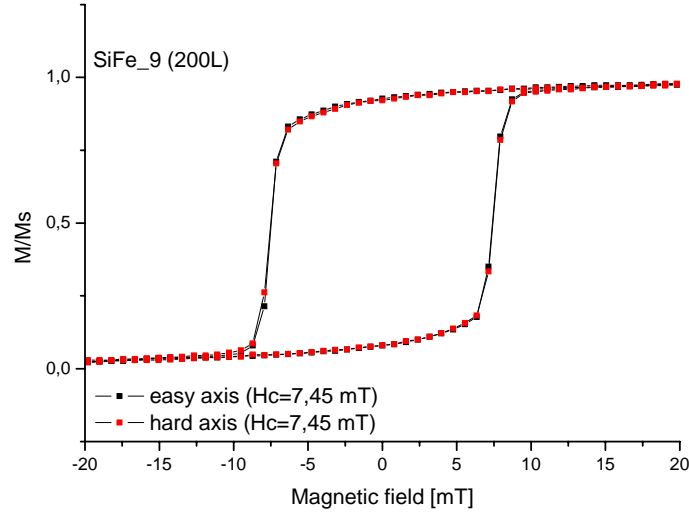


Fig.13 Hysteresis loops for the two axes. The oxygen exposure is 200L.

In the case of the sample with 100L oxide exposure (Fig. 14) the hysteresis loops look completely different. It can be explained by the small thickness of the oxide layer. The H_c for this sample is $H_{c(e.a.)}=3.55\text{mT}$, $H_{c(h.a.)}=2.05\text{mT}$.

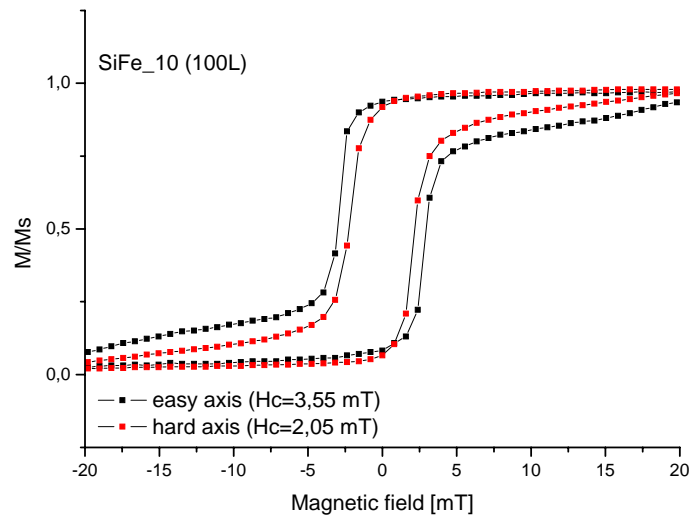


Fig.14 Hysteresis loops for the two axes. The oxygen exposure is 100L.

For the two last samples, the oxide exposure was 400L and 350L (Fig.15 and 16), but in this case we don't observe the effect like for samples SiFe_7 and SiFe_8 (Fig.11 and 12). The reason for that is not understood yet.

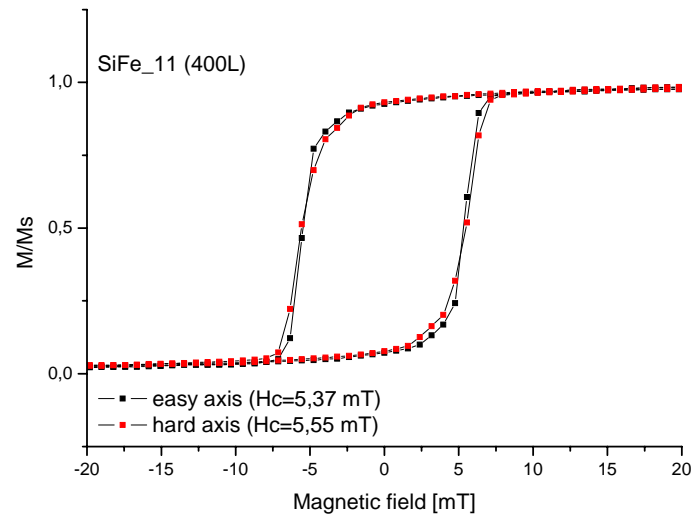


Fig.15 Hysteresis loops for the two axes. The oxygen exposure is 400L.

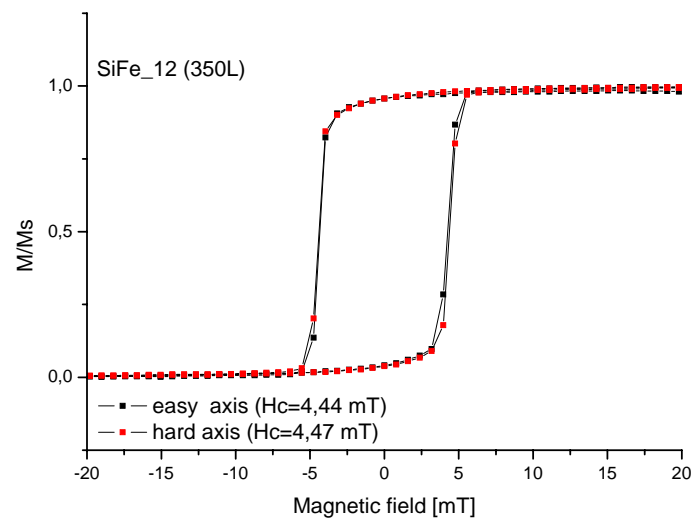


Fig.16 Hysteresis loops for the two axes. The oxygen exposure is 350L.

The last plot shows the dependence of the H_c on the exposure. We can see two peaks are found at 300-400L and 900L. There are no explanation for this effect now, and this question demand of subsequent study.

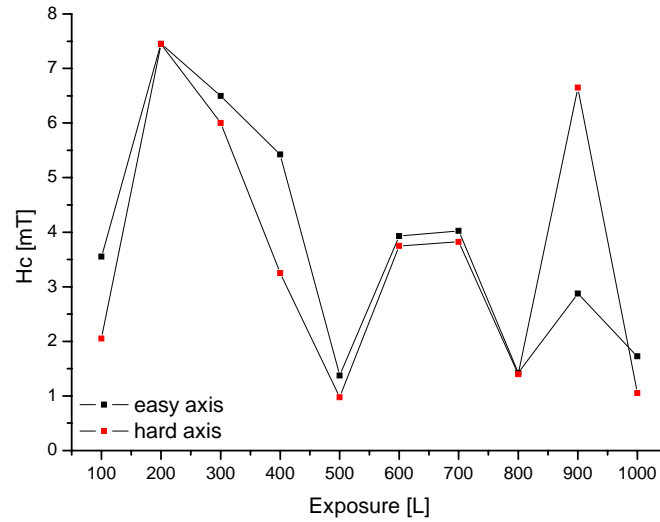


Fig.17 Evolution of the coercivity as a function of the oxygen exposure.

Conclusions.

In this work we investigate influence of the oxide thickness on the magnetic properties of the Fe/FeO multilayers. In area of the oxygen exposure 300-400L and 900L we have observed some switchings on hysteresis loops. This effect can be explained by the switching in domain structure of multilayer magnetic films. In future we want to continue the investigation this effects, changing sputtering and oxidation parameters.

References.

1. S. Couet, K. Schlage, K. Saksl, R. Röhlberger *How metallic Fe controls the composition of its native oxide*, Phys. Rev. Lett. 101, 066 101 (2008)
2. S. Couet, Th. Diederich, K. Schlage, R. Röhlberger *A compact UHV deposition system for in-situ study of ultrathin films via hard x-ray scattering and spectroscopy*, Rev. Sci. Inst. (2008)